



**HAL**  
open science

## Mannose-based surfactant as biofunctional nanoemulsion stabilizer

Pablo Argudo, Lea Spitzer, Emmanuel Ibarboure, François Jerome, Henri Cramail, Sébastien Lecommandoux

### ► To cite this version:

Pablo Argudo, Lea Spitzer, Emmanuel Ibarboure, François Jerome, Henri Cramail, et al.. Mannose-based surfactant as biofunctional nanoemulsion stabilizer. *Colloids and Surfaces B: Biointerfaces*, 2022, 220, pp.112877. 10.1016/j.colsurfb.2022.112877 . hal-03844794

**HAL Id: hal-03844794**

**<https://hal.science/hal-03844794v1>**

Submitted on 9 Nov 2022

**HAL** is a multi-disciplinary open access archive for the deposit and dissemination of scientific research documents, whether they are published or not. The documents may come from teaching and research institutions in France or abroad, or from public or private research centers.

L'archive ouverte pluridisciplinaire **HAL**, est destinée au dépôt et à la diffusion de documents scientifiques de niveau recherche, publiés ou non, émanant des établissements d'enseignement et de recherche français ou étrangers, des laboratoires publics ou privés.

1

# 2 Mannose-based surfactant as biofunctional

## 3 nanoemulsion stabilizer

4 *Pablo G. Argudo,<sup>1,‡,\*</sup> Lea Spitzer,<sup>1,2,‡</sup> Emmanuel Ibarboure,<sup>1</sup> François Jerome,<sup>2</sup> Henri Cramail,<sup>1</sup>*  
5 *Sébastien Lecommandoux,<sup>1,\*</sup>*

6 <sup>1</sup>Univ. Bordeaux, CNRS, Bordeaux INP, LCPO, 16 Avenue Pey-Berland, 33600 Pessac, France

7 <sup>2</sup>Institut de Chimie des Milieux et Matériaux de Poitiers, CNRS-Université Poitiers, ENSIP, 1 rue  
8 Marcel Doré, 86073 Poitiers, France

### 9 **Abstract**

10 The development and implementation of new amphiphiles based on natural resources rather than  
11 petrochemical precursors is an essential requirement due to their feedstock depletion and adverse  
12 environmental impacts. In addition, the use of bio-based surfactants can provide unique  
13 characteristics and improve the properties and versatility of the colloidal systems in which they are  
14 applied, such as emulsions. Here, the emulsification properties of a synthesized biocompatible  
15 mannose-based surfactant were investigated. Its behavior was evaluated in the presence of four  
16 different natural oils (castor, sunflower, olive and soybean) as well as two different aqueous phases  
17 (pure water and phosphate-buffered saline). The results highlighted their interest as surfactant in  
18 O/W nanoemulsions for all tested oil and aqueous phases, using a low-energy preparation protocol  
19 and relatively low surfactant concentrations. Furthermore, the mannose groups present on the polar  
20 head of the surfactant and adsorbed on the surface of the emulsion droplets were shown to retain  
21 their native biological properties. The specific mannose-concanavalin A binding was observed *in*

22 *vitro* by the designed nanoemulsions, revealing the biorecognition properties of the surfactant and  
23 its potential applicability as a nanocarrier.

24 **Keywords:** nanoemulsion, biorecognition, mannose, concanavalin A, particle size distribution

## 25 **1. Introduction**

26 Nanoemulsions are emulsions in the submicrometer range which can be described as a kinetically  
27 stable single-phase system with a droplet diameter in the 100 to 500 nm range[1–3]. In this kind of  
28 systems, the interface between two immiscible liquids is stabilized by the addition of a surface-  
29 active compound in low concentration, *e.g.* a surfactant. This results in a colloidal dispersion where  
30 the nature of the components will be directly related to the final properties of the system[4]. A wide  
31 range of emulsification methods can be used to produce different types of emulsions, including oil-  
32 in-water (O/W), water-in-oil (W/O), or even more complex multiple emulsions, *e.g.* oil-in-water-in  
33 oil (O/W/O) and water-in-oil-in-water (W/O/W) systems[5–7]. Extreme emulsification, phase  
34 inversion, nanofluidics, membrane emulsification or satellite droplets are only a few of the most  
35 extended methods used in their preparation[8]. With a stability from weeks to months,  
36 nanoemulsions are absent of any thermodynamic restrictions or specific temperature effects[9] that  
37 can limit their composition, in contrast to microemulsions, widening their use in drug delivery  
38 systems, food, cosmetics, templates or material synthesis[10]. However, new formulations that  
39 improve their properties as well as their ecological nature are on demand while maintaining a desired  
40 functionality and well-controlled physical properties[11]. Most of the currently in use emulsifiers  
41 have a petrochemical origin. Over the last few years, there is a gradual tendency in their substitution  
42 by biomolecules due to the petroleum feedstock decrease and its effect in the climate change[12].  
43 Among all the possible replacements, sugar-based surfactants have emerged as a commercially  
44 consistent alternative[13], particularly the ones based on monosaccharides acting as hydrophilic  
45 unit. Although they can be obtained from renewable raw materials, they add innate properties such  
46 as biodegradability, low toxicity and biocompatibility, thus meeting the principles of green

47 chemistry[14]. Out of all sugars, D-mannose is one of the most widely used in the food and  
48 biomedical fields[15]. Its properties allow it to be used as a novel transgene adjuvant to control  
49 chronic neuropathic pain[16], to reduce the risk of urinary tract infections[17], and more  
50 importantly, it can be used as an anchor point due to its specific recognition process with mannose-  
51 binding lectins (MBLs)[18]. Lectins are a promising tool for the detection of biomarkers, as bacteria  
52 or cancer cells, in bodily fluids and tissues[19]. Synthetic mannosylated systems have been recently  
53 synthesized[20] and used as vehicles to specifically deliver drugs or antigens to these cells, mostly  
54 in the form of vaccines[21,22]. Nevertheless, due to their multivalency, MBLs bind to high-order  
55 glycan structures while their affinity for monosaccharides units remains fairly low[23]. Monovalent  
56 mannose-based ligands, while able to yield good interactions with mannose receptors, lack the high  
57 affinities that multivalent ligands have, in agreement with the cluster effect that leads to more  
58 efficient targeting effects[24]. The design of synthetic ligands capable of recognizing glycoreceptors  
59 with high affinity and their incorporation to our daily uses is of vital importance.

60 In the present work, we report the development and applicability of an ecofriendly amphiphile  
61 characterized by a mannose-based polar head group and oleic acid tail as nonpolar moiety, (PMan)<sub>9</sub>-  
62 *b*-OI, as emulsifier. The branched polysaccharidic head of this surfactant was designed to improve  
63 its affinity to MBLs, while maintaining the innate features of the sugar while forming O/W  
64 nanoemulsions with vegetable oils. By dynamic light scattering, laser scanning confocal microscopy  
65 and turbidity experiments, the emulsion droplets and their stability were characterized. Furthermore,  
66 its applicability and biocompatibility properties were elucidated when selectively binding *in vitro*  
67 to concanavalin A, a MBL, showing the feasible use of this novel surfactant in the design of  
68 biological drug delivery systems, working as nanocarrier.

69

## 70 2. Materials and Methods

71 **2.1. Materials.** (PMan)<sub>9</sub>-*b*-OI surfactant (Propargyl-(oligo)-mannopyranoside-*b*-oleic-acid,  
72 mannose, Degree of Polymerization,  $\overline{DP} = 9$ ) was synthesized by our group. Olive oil (from *olivae*  
73 *oleum virginale*, >99%), castor oil (from *ricinus communis*, >99%) and sunflower seed oil (from  
74 *helianthus annuus*, >99%) were supplied from Sigma-Aldrich (St. Louis, MO, United States of  
75 America). Soybean oil (from *glycine max*, >99%) was purchased from Alfa Aesar (Havervill, MA,  
76 United States of America). Phosphate-buffered saline (PBS) 10x solution was obtained from  
77 Euromedex (Souffelweyersheim, France). CaCl<sub>2</sub> and MnCl<sub>2</sub>·4H<sub>2</sub>O salts were supplied by Sigma-  
78 Aldrich (St. Louis, MO, United States of America) and Alfa Aesar (Havervill, MA, United States  
79 of America), respectively. Nile Red dye, Concanavalin A (ConA, from *canavalia ensiformis*) and  
80 Ricinus Communis Agglutinin I (RCA<sub>120</sub>, from castor bean) lectins were purchased from Sigma-  
81 Aldrich (St. Louis, MO, United States of America). Ultrapure deionized water, used for cleaning  
82 and dispersion preparation, was obtained by a Millipore Milli-Q unit, and pretreated by a Millipore  
83 reverse osmosis system (>18.2MΩ cm<sup>-1</sup>).

84 **2.2. Nanoemulsion preparation.** Nanoemulsions were prepared by the weight (with a ± 0.1 mg  
85 precision) of the different compounds that form it. (PMan)<sub>9</sub>-*b*-OI was used as surfactant. Castor,  
86 soybean, sunflower, and olive oils were employed separately as oleic phases. Ultrapure deionized  
87 water as well as phosphate-buffered saline (PBS) (with 0.1 mM CaCl<sub>2</sub> and 0.1 mM MnCl<sub>2</sub>, pH =  
88 7.2) were used as aqueous phases. Thus, every nanoemulsion prepared is described in function of  
89 its amount of surfactant, water phase and oil phase used (expressed in wt%). The ratio between the  
90 compounds in each sample can be obtained from the respective ternary pseudo-phase diagram  
91 ((PMan)<sub>9</sub>-*b*-OI/Oil phase/Aqueous phase).

92 The protocol of preparation was as follows: first, the required amount of (PMan)<sub>9</sub>-*b*-OI was weighed  
93 and poured into a vial. Then, the aqueous phase was weighted and added, and the mixture was  
94 homogenized for 30 min using a magnetic stirrer (1000 rpm). Finally, oleic phase was also  
95 incorporated to the vial, leading to the final desired composition. The final ternary mixture was

96 homogenized for 24 h using a magnetic stirrer (1400 rpm) at room temperature (*e.g.*, a (PMan)<sub>9</sub>-b-  
97 OI/Soybean oil/PBS emulsion in a 5/25/70 wt% ratio was made by the stirring at 1000 rpm of 50  
98 mg of surfactant in 700 mg of a PBS solution. Then, 250 mg of soybean oil were added and the final  
99 mixture stirred at 1400 rpm for 24h). It is worth noting that specific stirring conditions, time, and  
100 speed motion during the preparation of the nanoemulsions were not required to obtain the final  
101 dispersions.

102 **2.3. Determination of the Nanoemulsion Region.** The boundary of the nanoemulsion region  
103 was analyzed at room (25 °C) and human physiological (37 °C) temperatures for the determination  
104 of the pseudo-ternary phase diagram. Every diagram corresponds to a cut of the whole ternary phase  
105 diagram at constant temperature and pressure, where the amount of (PMan)<sub>9</sub>-b-OI used varies  
106 between 1 and 5 wt%. The nanoemulsion regions were identified as those dispersions where a final  
107 homogeneous and stable one phase system was obtained during at least 14 days.

108 **2.4. Sample preparation protocol for emulsion-lectin recognition studies *in vitro*.** A 5/25/70  
109 wt% (PMan)<sub>9</sub>-b-OI/Soybean oil/PBS nanoemulsion at 37 °C was diluted in PBS in a 1:1000 ratio.  
110 For the DLS measurements, 200 µL of the diluted emulsion in PBS were taken out and 5 µl of a  
111 lectin (1 mg/ml in PBS) solution were added in an Eppendorf tube. The mixture was shaken at room  
112 temperature for 20 minutes before the lectin was incubated for 40 min at 37 °C under shaking.  
113 Finally, solutions were centrifuged at 37 °C for 20 min at 10,000 g. The supernatant was removed,  
114 and the residue redispersed in PBS buffer solution prior sample characterization. This washing step  
115 was repeated three times before the samples were measured by DLS. For LSCM measurements, the  
116 emulsions were loaded with Nile Red as follow : 200 µl of the diluted emulsion were loaded using  
117 20 µl of a 1 mg/mL Nile Red solution in methanol by magnetically stirring the mixture (750 rpm)  
118 for 30 min at room temperature. For turbidity measurements, 300 µL of a 0.016 mg/ml solution of  
119 the studied lectin (conA or RCA<sub>120</sub>) were added together with 200 µL diluted emulsion into a quartz  
120 cuvette and placed in a UV spectrometer.

121 **2.5. Dynamic light scattering.** DLS measurements were performed using two different setups  
122 depending on the concentration, transparency, and turbidity of the sample. Emulsions were  
123 characterized by a Vasco Particle Size Analyzer (Cordouan Technologies, Pessac, France) at 25 °C  
124 and 37 °C using a diode laser (wavelength,  $\lambda = 532$  nm) and a scattering angle  $\theta = 135^\circ$ . Based on  
125 enhanced DLS, turbid as well as opaque samples can be properly measured and characterized.  
126 Diluted samples were studied by a Zetasizer Nano ZS (Malvern Instruments Ltd., United Kingdom)  
127 at 25 °C and 37 °C using a He–Ne laser (wavelength,  $\lambda = 632$  nm) in a quasi-backscattering angle  $\theta$   
128  $= 173^\circ$ . In DLS experiments, it can be obtained the normalized intensity or second-order  
129 autocorrelation function,  $g^{(2)}(q,t)$ , which is directly related to the field or first-order autocorrelation  
130 function,  $g^{(1)}(q,t)$ , equation (1), where  $\beta$  is the optical factor with a value close to 1 [25]. In the case  
131 of a monodisperse sample describing a Brownian motion,  $g^{(2)}(q,t)$  can be defined in function of a  
132 single exponential decay. In this case, the diffusion coefficient can be related to the inverse of the  
133 decay time, equation (2), being  $q = (4\pi n/\lambda) \sin(\theta/2)$  and  $n$  the continuous phase refractive index  
134 ( $n = 1.33$ ). In Newtonian conditions, spherical particles, and their apparent hydrodynamic diameter,  
135  $d_{app}^H$ , can be obtained by the Stokes–Einstein relationship, equation (3), where  $k_B$  denotes the  
136 Boltzmann constant,  $T$  the temperature, and  $\eta$  is the viscosity.

$$g^{(2)}(q, t) - 1 = \beta |g^{(1)}(q, t)|^2 \quad (1)$$

$$D_{app} = 1/\tau q^2 \quad (2)$$

$$d_H^{app} = k_B T / 3\pi\eta D_{app} \quad (3)$$

137 **2.6. UV-Vis spectroscopy.** Turbidity experiments were carried out by a Cary 100 UV-Visible  
138 (Agilent Technologies, Santa Clara, CA, United States of America) at a fixed wavelength of 420  
139 nm. The dispersions were placed in a 0.5 mL and 10 mm path length quartz cuvette. Their  
140 absorbance evolution was followed in a time period of 60 min with a time step of 30 seconds. All  
141 protein aggregates scatter light in the visible wavelength region (400 - 700 nm) since their size  
142 ranges from nanometer to micrometer [26,27]. Turbidity experiments describe the attenuation of an

143 incident beam by light scattering in time due to protein aggregation reactions taking place. Thus,  
144 the emulsion-lectin interactions can be tracked.

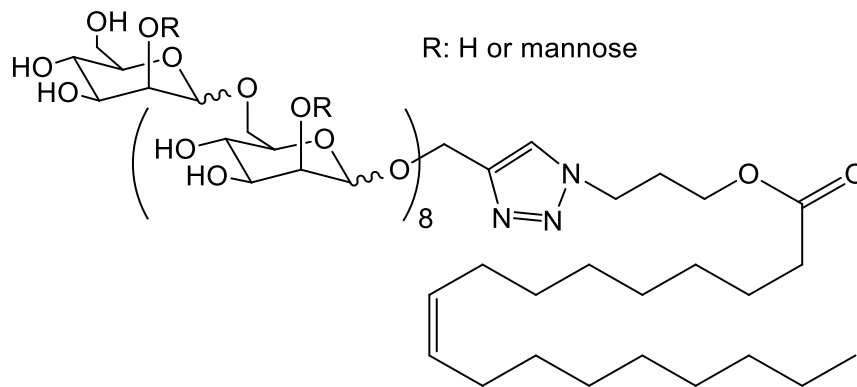
145 **2.7. Laser scanning confocal microscopy.** LSCM images were acquired on an inverted Leica  
146 TCS SP5 microscope equipped with a PL APO 0.4 10x air objective (Leica Camera, Wetzlar,  
147 Germany). 20  $\mu$ L samples were deposited on a planar glass substrate and covered in order to form  
148 a thin film prior analysis. The laser outputs were controlled via an Acousto-Optical Tunable Filter  
149 (AOTF) and the two collection windows using the Acousto-Optical Beam Splitter (AOBS) and  
150 photomultipliers (PMT) as follows: Nile Red was excited with a DPPS diode at 561 nm (15 %)  
151 and measured with emission setting at 565 - 600 nm. Aggregates were excited with a He-Ne laser  
152 at 633 nm (10 %) in transmission mode. Images were collected using the microscope in sequential  
153 mode with a line average of 16.

### 154 **3. Results and discussion**

155 The main objective of this study was to characterize the emulsifying and biological recognition  
156 properties of an engineered sugar-based surfactant. The molecular structure of the amphiphile is  
157 based on a mannose oligosaccharide polar head group linked to a hydrophobic oleic acid tail by  
158 “click chemistry”, **Figure 1**. The synthesis procedure and characterization of the mannlipid,  
159 denoted as (PMan)<sub>9</sub>-*b*-OI, is described in **SI.1**. A comprehensive overview of the synthesis  
160 procedure of similar sugar-based amphiphiles has already been reported[28]. In brief, the surfactant  
161 is described as having a mannose-based polar head group with a high average degree of  
162 polymerization,  $\overline{DP} = 9$ , and a dispersity,  $\mathcal{D} = 2$ , as expected for a polycondensation synthesis. Most  
163 of the monosaccharide units are linearly connected via  $\alpha$ -(1,6)-linkages along with a partial presence  
164 of  $\alpha$ -(1,2)-linkages, leading to its final branched pattern. Thus, the polar head group, (PMan)<sub>9</sub>, can  
165 be depicted as a long sugar-based branched moiety with free D-(+)-Mannose terminal sugars. The  
166 final nonionic surfactant is characterized as a mainly hydrophilic molecule, with a theoretical



167 average hydrophilic-lipophilic balance, HLB, of 15, which tends to form oil-in-water (O/W)  
168 emulsions[29].



169  
170 **Figure 1.** Molecular structure of the mannolipid. R denotes the  $\alpha$ -(1,2) mannose ramification  
171 position.

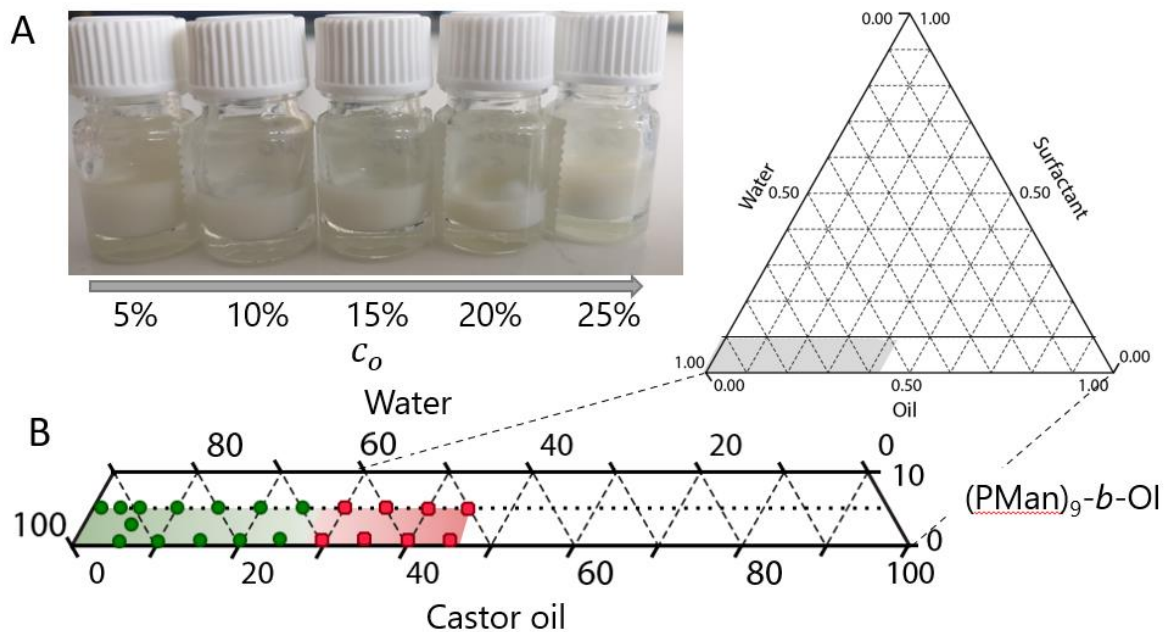
172

### 173 3.1. Determination and characterization of the nanoemulsion region.

174 A preliminary step, in connection with the use of O/W nanoemulsions as active carriers, is the  
175 determination of the composition range in which nanoemulsions are formed. As starting point, the  
176 nanoemulsions were studied under simplified conditions to further determine the effects of PBS and  
177 temperature on the system. Using a pseudo-ternary phase diagram, different (PMan)<sub>9</sub>-*b*-  
178 OI/Oil/Water ratios were tested at a fixed temperature of 25°C. A set of different vegetable oils  
179 (castor, sunflower, olive, and soybean) with similar nature to the hydrophobic region of the  
180 surfactant were studied in order to increase the stability of the emulsion.[25] Emulsions based on  
181 vegetable oils are easily accessible and biocompatible with and extended use in our daily uses.  
182 Castor oil as oil phase is used to obtain oil-in-water nanoemulsions capable of successfully  
183 solubilizing quercetin, a natural polyphenol occurring in anti-inflammatory, antibacterial,  
184 antioxidant, antiangiogenic, and antitumor activities,[26] while sunflower seed oil is used to  
185 encapsulate of both hydrophilic (i.e., iron oxide nanoparticles) and lipophilic (i.e., rhodamine B or  
186 epirubicin) materials.[26] Considering the applicability of the emulsion, the pseudo-ternary phase  
187 diagram was a cutoff of the true phase diagram containing a maximum concentration of (PMan)<sub>9</sub>-

188 *b*-OI,  $c_s$ , of 5 wt%. Compared to microemulsions, low  $c_s$  are used in nanoemulsions to reduce their  
 189 toxicity[30]. In addition, the total concentration of the oil phase,  $c_o$ , was considered to be in the  
 190 range of 0 – 45 wt%. Beyond this concentration, the oil would be the main phase present in the  
 191 system, which would make impossible the use of the O/W nanoemulsion term.

192 In all (PMan)<sub>9</sub>-*b*-OI/Oil/Water systems tested, nanoemulsions were obtained when the surfactant  
 193 and oil concentrations ranged between 0.5–5 and 1–25 wt%, respectively. While stable  
 194 nanoemulsions were obtained at all tested  $c_s$ , at  $c_o$  above 25 wt%, most of the dispersions were  
 195 unstable. They were characterized by a clear phase separation in which the two main liquid  
 196 constituent components used, aqueous and oleic, split after a creaming process. **Figure 2** shows  
 197 characteristics photos of the samples and the ternary phase diagram of (PMan)<sub>9</sub>-*b*-OI/Castor  
 198 oil/Water, as example. As it can be seen, although stable in the  $c_s$  range of 1 to 5 wt%, no turbidity  
 199 changes are observed when the  $c_o$  is varied up to 25 wt%, maintaining its milky appearance.



200

201 **Figure 2.** (a) Photos of the dispersions of (PMan)<sub>9</sub>-*b*-OI/Castor oil/Water emulsions increasing the  
 202 castor oil ratio from left to right at a fixed 5 wt% of surfactant. (b) Ternary phase diagram  
 203 representing a cut of the whole phase wt% diagram obtained at 25°C for the (PMan)<sub>9</sub>-*b*-OI/Castor  
 204 oil/Water system. Studied oil-in-water (O/W) nanoemulsion region is evidenced in gray. Stable and

205 unstable O/W nanoemulsions are denoted by green and red dots, respectively. Notice that the axes  
206 represent the wt% of every component.

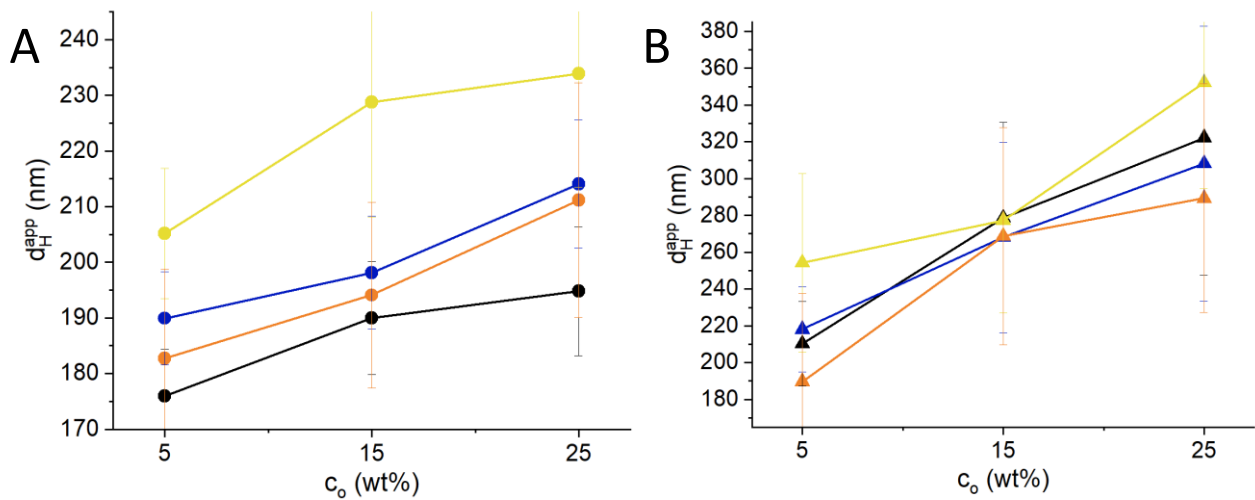
207

208 Moreover, similar results were obtained for other dispersed phases, such as sunflower, olive, and  
209 soybean oils. **SI.2** shows the photos and the ternary phase diagrams of each oil with each sample  
210 composition tested. The stability of the nanoemulsions can be related to the chemical structure of  
211 these natural oils, based on different ratios of ricinoleic, palmitic, oleic, linoleic and linolenic acid,  
212 in line with the hydrophobic tail of the surfactant. (PMan)<sub>9</sub>-*b*-OI, as a nonionic surfactant, mainly  
213 promotes the stabilization by steric repulsions, limiting the molecular approach to the fluid interface.  
214 The mannose-based polar head is faced to the continuous aqueous media while the hydrophobic  
215 oleic-based tail does it to the oleic one. In this way, the surfactant is positioned as a steric barrier,  
216 reducing the surface tension and increasing its elasticity, preventing fluctuations that could lead to  
217 coalescence processes. While a bulky hydrophilic moiety is relevant as a steric barrier, as in  
218 (PMan)<sub>9</sub>, so is the structure of the hydrophobic one. A difference in the chemical structure of the  
219 lipophilic tail respect to the oil clearly affects the stabilization of the nanoemulsion. Consequently,  
220 mineral oil, characterized by saturated and aromatic structures, led to phase separation, **SI.2**.

221 While in an aqueous media surfactants with similar molecular structure self-assemble into micelles  
222 with mean hydrodynamic diameter values,  $d_H^{app}$ , of *c.a.* 10 nm,[31] when used in an emulsified  
223 system, (PMan)<sub>9</sub>-*b*-OI form droplets characterized  $d_H^{app}$  of *ca.* 160 to 350 nm, depending on the oil  
224 and surfactant concentrations. All the O/W nanoemulsions denoted an average PDI of *ca.* 0.2 and a  
225 minimum stability of 14 days at room temperature, as indicated by DLS. **SI.3** collects each  $d_H^{app}$   
226 value over time for each sample. As expected, a direct relationship between the oil:water and  
227 surfactant:oil ratios was observed in the final size of the nanoemulsion. At a constant (PMan)<sub>9</sub>-*b*-OI  
228  $c_s$  of 1 wt%, an increase in the oil:water ratio leads to higher  $d_H^{app}$  values, **Figure 3a**. A constant  
229 amount of surfactant molecules are available to cover a higher amount of oleic phase. Therefore,

230 the extra amount of oil must be redistributed in the system, namely inside the droplets, which leads  
231 to an increase in droplet size. When this ratio increases and a  $c_o$  of 30 wt% is reached, irrespective  
232 of the type of oil, the system becomes unstable and the emulsion phase separates. Same  $d_H^{app}$  trend  
233 was observed for similar oil:water ratios when the  $c_s$  was increased to 5 wt%, **Figure 3b**. However,  
234 the use of larger amount of surfactant seems to have no effect or slightly increase the  $d_H^{app}$  and  
235 polydispersity of the droplets. Note that, in the case of simple surfactants, an increase in  $c_s$  is  
236 associated to a decrease in the average droplet size. A higher surfactant concentration allows the oil  
237 droplets to be more dispersed while remaining coated, which reduces the surface tension of the  
238 smaller droplets[32]. (PMan)<sub>9</sub>-*b*-OI, due to its complex molecular structure and the unique behavior  
239 of sugar-derivatives at interfaces, can undergo an assembly reorganization at the interface as  
240 function of its concentration. Complex hydrophobic tails have been reported to adopt different  
241 configurations depending on the system, such as bent or linear [33,34]. Also, it is known that sugar-  
242 sugar hydrogen bonding interactions can also play a key role in the self-assembly processes and the  
243 final conformation[35]. Finally, taking into account that non-constant water:oil ratios were used at  
244 fixed  $c_s$ , it is impossible to accurately compare and explain the effect of the surfactant concentration  
245 on the final average size distribution. *E.g.*, 1/25/74 and 5/25/70 wt% (PMan)<sub>9</sub>-*b*-OI/Olive oil/Water  
246 emulsions are described by 2.96 and 2.8 water:oil ratios, respectively. Nevertheless, as the  
247 delimitation of the stable emulsification region was the main objective of the work, further  
248 rheological studies are suggested to explain this behavior. Regarding stability, no coalescence was  
249 observed after 14 days. A minimal increase in the  $d_H^{app}$  and PDI was observed, demonstrating that

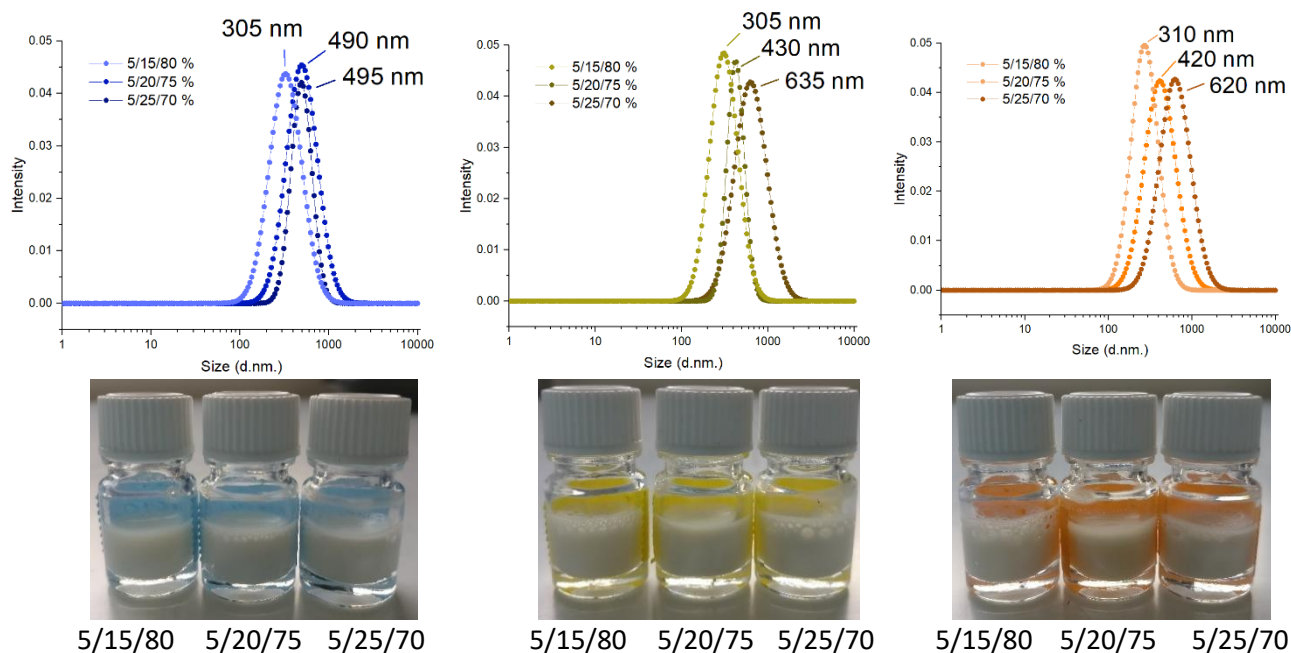
250 the O/W nanoemulsion droplets are quite stable against coalescence, while a phase separation starts  
251 to occur after several weeks.



252 **Figure 3.** Average droplet size distribution of castor (●,▲), sunflower (●,▲), soybean (●,▲) and  
253 olive (●,▲) oil (PMan)<sub>9</sub>-*b*-OI/oil/water nanoemulsions at 25 °C with (a) 1 wt% and (b) 5 wt%  $c_s$ .

254  
255 Considering the applicability of the emulsion, the aqueous medium of the system was replaced by  
256 PBS at pH 7.2 and analysed at 37 °C to approximate biological conditions. Nanoemulsions with a  
257  $c_s$  of 5 wt% and  $c_o$  in the 15 to 25 wt% region were studied, with no visual changes observed in the  
258 samples respect their continuous pure water counterparts, denoting their viability in this phosphate-  
259 buffered saline medium. Compared to water-based nanoemulsions, the addition of salts to the  
260 system and the increase in temperature raised the average droplet size, as shown in **Figure 4**.  
261 Although stable, the  $d_H^{app}$  values obtained in PBS increased in the  $c_o$  15 to 25 wt% range, compared  
262 to MilliQ water-based nanoemulsions, leading to O/W nanoemulsion droplets of *ca.* 200 to 450 nm  
263  $d_H^{app}$ . This variation in droplet size is expected. Although the assembly of nonionic surfactants is  
264 less affected by ionic strengths and pH changes compared to ionic ones at the time of stabilizing  
265 interfaces, changes in the temperature can affect the system stability and surface-tension[36]. It is  
266 known that the presence of sodium phosphate increases the surface tension with respect to pure  
267 water, destabilizing the interface, promoting the coalescence and therefore the final increase of

268  $d_H^{app}$ . Moreover, a direct relationship between the  $c_o$  and  $d_H^{app}$  was also observed, as previously in  
 269 aqueous media, where an increase of the oil wt%, while decreasing the continuous phase wt%, also  
 270 led to a final increase in droplet size.



271 **Figure 4.** Average droplet size distribution of sunflower (●), soybean (●), and olive oil (●)  
 272 (PMan)<sub>9</sub>-b-OI/oil/PBS nanoemulsions at 37 °C with a  $c_s$  5 wt%.

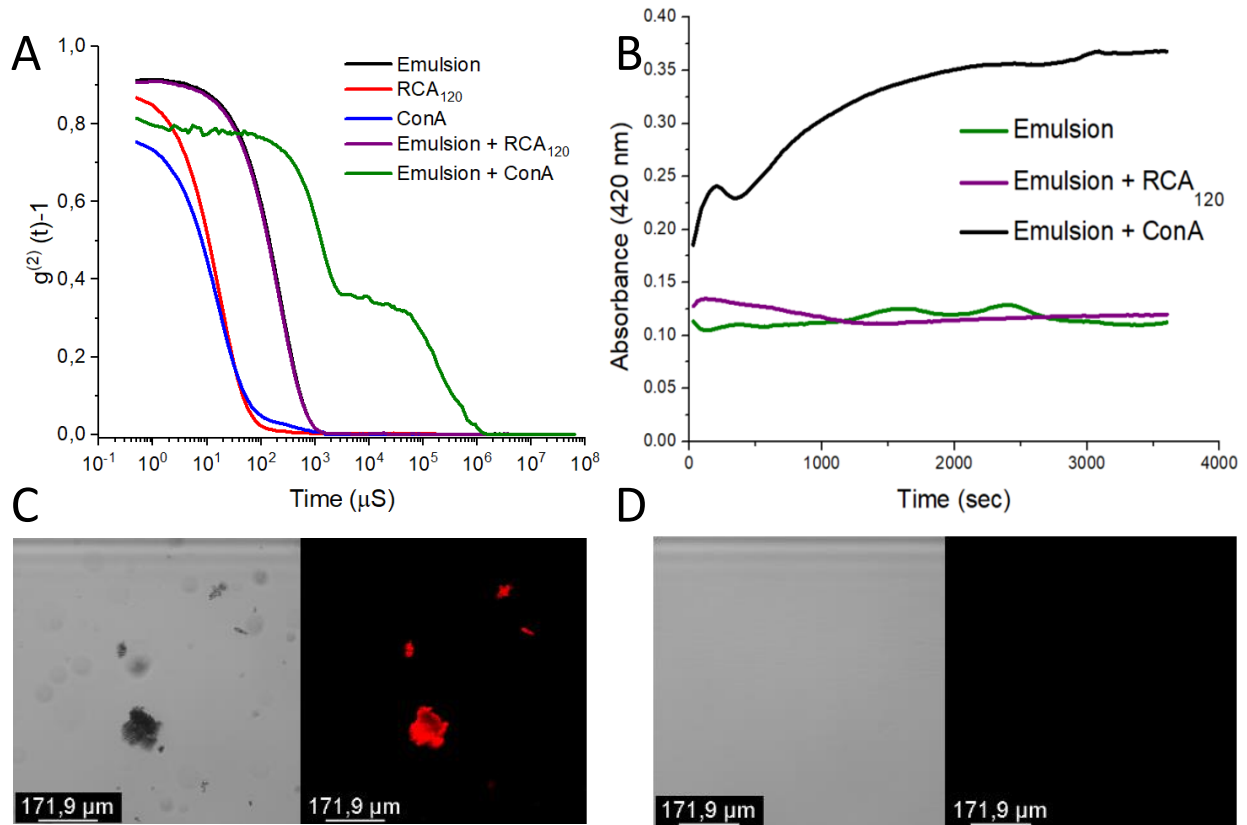
273

### 274 3.2. Protein recognition specificity.

275 As a proof of concept, the recognition properties of the nanoemulsion, and specifically of the  
 276 designed mannose-based surfactant, were studied under *in vitro* conditions. The behavior of a  
 277 1:1000 diluted O/W emulsion of (PMan)<sub>9</sub>-b-OI/Soybean oil/PBS (5/25/70 wt%) at 37 °C was  
 278 studied after 30 min in the presence of two lectins: Concanavalin A, ConA, and Ricinus Communis  
 279 Agglutinin I, RCA<sub>120</sub>. ConA is a lectin known to bind to the monosaccharides D-mannose and D-  
 280 glucose [37], whereas RCA<sub>120</sub> only binds to galactose derivatives[38]. ConA is used as a first *in*  
 281 *vitro* test of cellular recognition processes due to its binding properties to various cell membrane  
 282 receptors. As a tetravalent ligand, it has four binding sites that, upon activation in the presence of

283 calcium, can bind up to a total of four D-mannose molecules. By DLS, the multivalent binding of  
 284 the mannose groups present in the emulsion droplet shell and the ConA can be tracked. In addition,  
 285 a direct effect of the lectin on the emulsified system could be observed, **Figure 5a**.

286



287

288 **Figure 5. (a)** Intensity auto-correlation functions for the  $(\text{PMan})_9\text{-}b\text{-OI/soybean oil/PBS}$  emulsion,  
 289 lectins and their mixture. **(b)** Absorbance in time of the  $(\text{PMan})_9\text{-}b\text{-OI/soybean oil/PBS}$  emulsion  
 290 alone and in presence of the lectins. **(c)**  $(\text{PMan})_9\text{-}b\text{-OI/soybean oil/PBS}$  emulsion in the presence  
 291 of ConA and **(d)**  $\text{RCA}_{120}$ .

292

293 While the diluted O/W emulsion of  $(\text{PMan})_9\text{-}b\text{-OI/Soybean oil/PBS}$  denoted a monomodal  
 294 distribution with a maximum in the 250 nm diameter range, in line with the previous more  
 295 concentrated samples, a shift to higher times was obtained when ConA was added to the medium.  
 296 Note that ConA and  $\text{RCA}_{120}$  are described by an assembly similar to biological conditions, where

297 their shape can be described in form of small individual colloidal particles, as shown by their  
298 respective auto-correlation functions[39,40]. In Brownian motion conditions, a longer time  
299 corresponds to larger objects or colloids in solution. As expected, the terminal mannose groups of  
300 the polar head of the surfactant interact with the lectin, which can also bind to more monosaccharide  
301 units due to its multivalency, leading to the formation of random aggregates. Due to this cascading  
302 interaction, aggregates were formed on a wide size scale. In contrast, in the presence of RCA<sub>120</sub> no  
303 change in the auto-correlation function was observed with respect to the starting emulsion system,  
304 concluding the absence of any interaction between the emulsion droplets and the lectin. To further  
305 confirm the specific binding of the (PMan)<sub>9-b</sub>-OI based emulsion, turbidity experiments were  
306 carried out, **Figure 5b**. PBS solutions of each lectin were added to a O/W emulsion of (PMan)<sub>9-b</sub>-  
307 OI/Soybean oil/PBS and their absorbance was measured in time. This method is commonly used  
308 for the binding determination between glycosides and lectins[41]. Lectin-emulsion aggregates  
309 scatter light in the visible wavelength region, resulting a change of turbidity. Consequently, the  
310 formation of aggregates can be directly observed by an increase in light absorbance. As it could be  
311 observed, the emulsion in presence of ConA led to their biological recognition and final formation  
312 of aggregates, as denoted by the increase in absorbance over time. On the other hand, the presence  
313 of RCA<sub>120</sub> denoted no hallmark of aggregation, characterized by a constant absorbance in time  
314 within the error as in the (PMan)<sub>9-b</sub>-OI/Soybean oil/PBS emulsion alone. Note that the first peak  
315 present in the emulsion sample in presence of ConA is related to the experimental set-up. The ConA  
316 solution was added on top of the emulsion sample while no stirring and thus no homogenization of  
317 the system was applied. A direct view of the final aggregates formed by the mannose-ConA binding  
318 process was obtained by LSCM. A 1:1000 diluted 5/25/70 wt% (PMan)<sub>9-b</sub>-OI/Soybean oil/PBS  
319 nanoemulsion was loaded with a lipid-soluble fluorescent dye, Nile Red, which allowed the tracking  
320 of the droplets by fluorescence without affecting the  $d_H^{app}$  of the emulsion or its stability, **SI.4a**.  
321 Consistent with DLS and turbidity results, aggregates were observed in the  $\mu\text{m}$  range when the O/W



322 emulsion was in presence of ConA, **Figure 5c** and **SI.4b**. Note that only focused aggregates could  
323 be properly excited and characterized by fluorescence. However, when in the presence of the  
324 negative control, RCA<sub>120</sub>, no aggregation-induced effect was observed due to the absence of any  
325 mannose-RCA<sub>120</sub> interaction, **Figure 5d**.

326

#### 327 **4. Conclusions**

328 We have successfully developed the formulation and application of an environmentally friendly  
329 amphiphile based on a mannose oligosaccharide polar head group and a hydrophobic oleic acid tail.  
330 At lower concentrations, in the range of 1 to 5 wt%, the designed surfactant forms stable O/W  
331 nanoemulsions for at least 14 days. Capable of dispersing natural oils such as castor, sunflower,  
332 olive, and soybean up to a 25 wt%, the final emulsion droplets are characterized by hydrodynamic  
333 sizes in the *ca.* 160 to 350 nm diameter range, depending on the oil and surfactant concentrations,  
334 using water at 25 °C as aqueous media. Under buffer conditions and at 37 °C, the size distribution  
335 of the nanoemulsions droplets increases to the *ca.* 200 to 450 nm range, as explained by the  
336 temperature increase and the present of salts that can destabilize the interface and promote droplet  
337 coalescence. In addition, the O/W nanoemulsions retained the specific biorecognition nature of the  
338 sugar. *In vitro* studies evidence how the mannose residues bind to ConA proteins, a lectin similar to  
339 human cellular membrane receptors, as MBL[42]. DLS, turbidity and LSCM experiments denote  
340 their interaction and cluster formation. Due to the branching of the surfactant and the multivalency  
341 of ConA a cascade binding reaction occurs and aggregates are formed from the emulsion droplets  
342 and lectin. The surfactant used in the present work opens a new route to produce biofriendly  
343 amphiphiles that could replace chemical surfactants for biological recognition processes and future  
344 drug delivery applications, as similar sugar-based surfactants that worked under the same *in vitro*  
345 conditions proposed here also did it *in cellulo*.[43] Novel mannose-based surfactants could be  
346 synthesized to target alveolar macrophages[40]. Not only focused on D-(+)-Mannose, other sugars

347 could also be envisioned to target additional receptors. Galactose-based ones could be developed  
348 for the recognition of Ricinus Communis Agglutinin, RCA<sub>120</sub>,<sup>[44]</sup> while fucose derivatives would  
349 bind to Ulex europaeus agglutinin lectin<sup>[45]</sup>, both with further applications in fungal and herbal  
350 environments, respectively.

351

## 352 **Associated Content**

353 Supporting Information. MALDI-TOF and <sup>1</sup>H NMR spectra of (PMan)<sub>9</sub>. Synthesis protocol and <sup>1</sup>H  
354 NMR spectra of (PMan)<sub>9</sub>-*b*-OI. Average droplet size and photos of (PMan)<sub>9</sub>-*b*-OI/oil phase/aqueous  
355 phase systems. Confocal images of ConA recognition experiments. The following files are available  
356 free of charge: Supporting\_Information (PDF)

## 357 **Author Information**

358 Corresponding Author

359 \* pgomezargud@enscbp.fr (P. A.)

360 \* Sebastien.Lecommandoux@enscbp.fr (S. L.)

361 Author Contributions

362 The manuscript was written through contributions of all authors. All authors have given approval to  
363 the final version of the manuscript. ‡These authors contributed equally.

## 364 **ORCID**

365 Pablo G. Argudo - [0000-0001-5964-727X](https://orcid.org/0000-0001-5964-727X)

366 Lea Spitzer - [0000-0002-0530-1262](https://orcid.org/0000-0002-0530-1262)

367 Emmanuel Ibarboure - [0000-0001-8614-3851](https://orcid.org/0000-0001-8614-3851)

368 François Jerome - [0000-0002-8324-0119](https://orcid.org/0000-0002-8324-0119)

369 Henri Cramail - [0000-0001-9798-6352](https://orcid.org/0000-0001-9798-6352)

370 Sébastien Lecommandoux - [0000-0003-0465-8603](https://orcid.org/0000-0003-0465-8603)

## 371 **Acknowledgment**

372 P.G.A., L.S., E.I., H.C., S.L. acknowledge the Centre National de la Recherche Scientifique, the  
373 Région Nouvelle Aquitaine, and the Université de Bordeaux. F.J. is thankful to the Université de  
374 Poitiers.

## 375 **References**

- 376 [1] T. Sheth, S. Seshadri, T. Prileszky, M.E. Helgeson, Multiple nanoemulsions, *Nat. Rev.*  
377 *Mater.* 5 (2020) 214–228. <https://doi.org/10.1038/s41578-019-0161-9>.
- 378 [2] J.M. Gutiérrez, C. González, A. Maestro, I. Solè, C.M. Pey, J. Nolla, Nano-emulsions: New  
379 applications and optimization of their preparation, *Curr. Opin. Colloid Interface Sci.* 13  
380 (2008) 245–251. <https://doi.org/10.1016/j.cocis.2008.01.005>.
- 381 [3] M.M. Fryd, T.G. Mason, Advanced nanoemulsions, *Annu. Rev. Phys. Chem.* 63 (2012)  
382 493–518. <https://doi.org/10.1146/annurev-physchem-032210-103436>.
- 383 [4] A. Ostróżka-Cieślik, B. Sarecka-Hujar, The Use of Nanotechnology in Modern  
384 Pharmacotherapy, *Multifunct. Syst. Comb. Deliv. Biosensing Diagnostics.* (2017) 139–158.  
385 <https://doi.org/10.1016/b978-0-323-52725-5.00007-1>.
- 386 [5] V.K. Rai, N. Mishra, K.S. Yadav, N.P. Yadav, Nanoemulsion as pharmaceutical carrier for  
387 dermal and transdermal drug delivery: Formulation development, stability issues, basic  
388 considerations and applications, *J. Control. Release.* 270 (2018) 203–225.  
389 <https://doi.org/10.1016/j.jconrel.2017.11.049>.
- 390 [6] Z. Zhi, R. Liu, W. Wang, K. Dewettinck, F. Van Bockstaele, Recent progress in oil-in-  
391 water-in-oil (O/W/O) double emulsions, *Crit. Rev. Food Sci. Nutr.* (2022) 1–12.  
392 <https://doi.org/10.1080/10408398.2022.2029346>.
- 393 [7] I. Klojdová, J. Štětina, Š. Horáčková, W/O/W Multiple Emulsions as the Functional

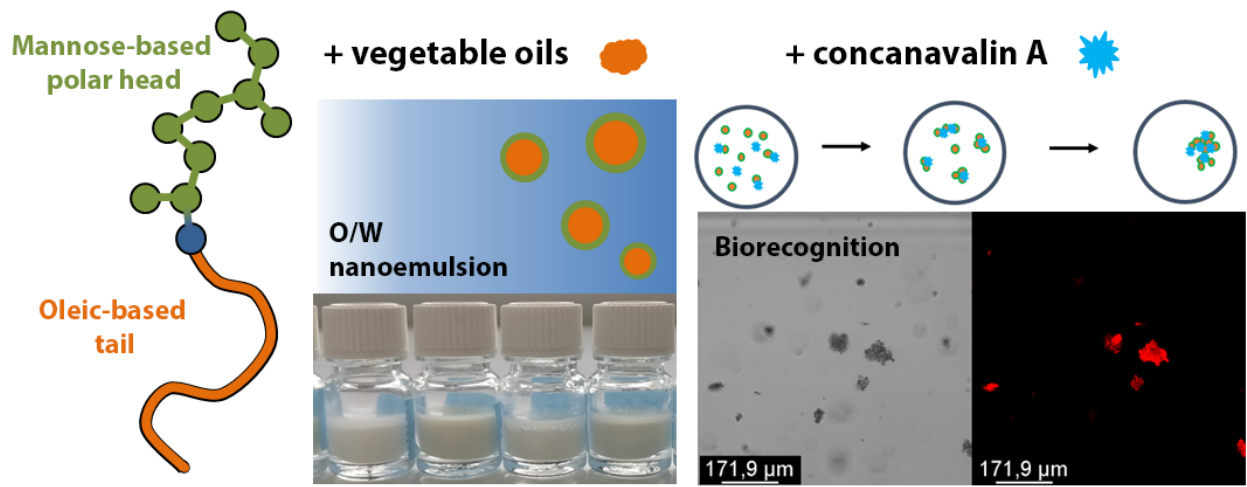
- 394 Component of Dairy Products, *Chem. Eng. Technol.* 42 (2019) 715–727.  
395 <https://doi.org/10.1002/ceat.201800586>.
- 396 [8] M.Y. Koroleva, E. V Yurtov, Nanoemulsions: the properties, methods of preparation and  
397 promising applications, *Russ. Chem. Rev.* 81 (2012) 21–43.  
398 <https://doi.org/10.1070/rc2012v081n01abeh004219>.
- 399 [9] R.B. Patel, M.R. Patel, S.D. Thakore, B.G. Patel, Nanoemulsion as a Valuable  
400 Nanostructure Platform for Pharmaceutical Drug Delivery, *Nano- Microscale Drug Deliv.*  
401 *Syst. Des. Fabr.* (2017) 321–341. <https://doi.org/10.1016/B978-0-323-52727-9.00017-0>.
- 402 [10] A. Gupta, H.B. Eral, T.A. Hatton, P.S. Doyle, Nanoemulsions: Formation, properties and  
403 applications, *Soft Matter*. 12 (2016) 2826–2841. <https://doi.org/10.1039/c5sm02958a>.
- 404 [11] D.G. De Almeida, R. de C.F. Soares Da Silva, J.M. Luna, R.D. Rufino, V.A. Santos, I.M.  
405 Banat, L.A. Sarubbo, Biosurfactants: Promising molecules for petroleum biotechnology  
406 advances, *Front. Microbiol.* 7 (2016) 1–14. <https://doi.org/10.3389/fmicb.2016.01718>.
- 407 [12] D. Welsby, J. Price, S. Pye, P. Ekins, Unextractable fossil fuels in a 1.5 °C world, *Nature*.  
408 597 (2021) 230–234. <https://doi.org/10.1038/s41586-021-03821-8>.
- 409 [13] C.F. Jesus, A.A.S. Alves, S.M. Fiuza, D. Murtinho, F.E. Antunes, Mini-review: Synthetic  
410 methods for the production of cationic sugar-based surfactants, *J. Mol. Liq.* 342 (2021)  
411 117389. <https://doi.org/10.1016/j.molliq.2021.117389>.
- 412 [14] C.C. Ruiz, *Sugar-Based Surfactants: Fundamentals and Applications*, 1st ed., CRC Press,  
413 2008.
- 414 [15] X. Hu, Y. Shi, P. Zhang, M. Miao, T. Zhang, B. Jiang, d-Mannose: Properties, Production,  
415 and Applications: An Overview, *Compr. Rev. Food Sci. Food Saf.* 15 (2016) 773–785.  
416 <https://doi.org/10.1111/1541-4337.12211>.
- 417 [16] E.C. Dengler, L.A. Alberti, B.N. Bowman, A.A. Kerwin, J.L. Wilkerson, D.R. Moezzi, E.  
418 Limanovich, J.A. Wallace, E.D. Milligan, Improvement of spinal non-viral IL-10 gene  
419 delivery by D-mannose as a transgene adjuvant to control chronic neuropathic pain, *J.*  
420 *Neuroinflammation*. 11 (2014) 1–21. <https://doi.org/10.1186/1742-2094-11-92>.
- 421 [17] R. Milandri, T. Bocchialini, M. Maltagliati, M. Cotugno, E. Simonetti, S. Ferretti, U.V.  
422 Maestroni, B.M.C. Rocco, S. Micali, Effects of D-Mannose, Ellirose<sup>TM</sup> and lactobacillus  
423 plantarum in treatment of urinary tract recurrent infections (rUTIs): A survey of urologists

- 424 knowledge about its clinical application, *Acta Biomed.* 91 (2020) 15–20.  
425 <https://doi.org/10.23750/abm.v91i1.8607>.
- 426 [18] C. Auriti, G. Prencipe, M. Moriondo, I. Bersani, C. Bertaina, V. Mondì, R. Inglese,  
427 Mannose-Binding Lectin: Biologic Characteristics and Role in the Susceptibility to  
428 Infections and Ischemia-Reperfusion Related Injury in Critically Ill Neonates, *J. Immunol.*  
429 *Res.* 2017 (2017). <https://doi.org/10.1155/2017/7045630>.
- 430 [19] O.H. Hashim, J.J. Jayapalan, C.S. Lee, Lectins: An effective tool for screening of potential  
431 cancer biomarkers, *PeerJ.* 2017 (2017) 1–30. <https://doi.org/10.7717/peerj.3784>.
- 432 [20] S. Cecioni, A. Imberty, S. Vidal, Glycomimetics versus multivalent glycoconjugates for the  
433 design of high affinity lectin ligands, *Chem. Rev.* 115 (2015) 525–561.  
434 <https://doi.org/10.1021/cr500303t>.
- 435 [21] N. Kojima, L. Biao, T. Nakayama, M. Ishii, Y. Ikehara, K. Tsujimura, Oligomannose-  
436 coated liposomes as a therapeutic antigen-delivery and an adjuvant vehicle for induction of  
437 in vivo tumor immunity, *J. Control. Release.* 129 (2008) 26–32.  
438 <https://doi.org/10.1016/j.jconrel.2008.03.023>.
- 439 [22] M.J. Copland, M.A. Baird, T. Rades, J.L. McKenzie, B. Becker, F. Reck, P.C. Tyler, N.M.  
440 Davies, Liposomal delivery of antigen to human dendritic cells, *Vaccine.* 21 (2003) 883–  
441 890. [https://doi.org/10.1016/S0264-410X\(02\)00536-4](https://doi.org/10.1016/S0264-410X(02)00536-4).
- 442 [23] C.P. Swaminathan, N. Surolia, A. Surolia, Role of water in the specific binding of mannose  
443 and manno oligosaccharides to concanavalin A, *J. Am. Chem. Soc.* 120 (1998) 5153–5159.  
444 <https://doi.org/10.1021/ja9733696>.
- 445 [24] S. Espuelas, C. Thumann, B. Heurtault, F. Schuber, B. Frisch, Influence of ligand valency  
446 on the targeting of immature human dendritic cells by mannosylated liposomes, *Bioconjug.*  
447 *Chem.* 19 (2008) 2385–2393. <https://doi.org/10.1021/bc8002524>.
- 448 [25] B.J.. Berne, R. Pecora, *Dynamic Light Scattering with Applications to Chemistry, Biology,*  
449 *and Physics, Inc.*, Pub, New York, USA, 2003.  
450 <https://doi.org/https://doi.org/10.1021/ed054pA430.1>.
- 451 [26] C.F. Bohren, D.R. Huffman, *Absorption and Scattering of Light by Small Particles*, Wiley,  
452 1998. <https://doi.org/10.1002/9783527618156>.
- 453 [27] M. Elimelech, J. Gregory, X. Jia, R.A. Williams, *Particle Deposition & Aggregation*,

- 454 Elsevier, 1995. <https://doi.org/10.1016/B978-0-7506-7024-1.X5000-6>.
- 455 [28] L. Spitzer, S. Lecommandoux, H. Cramail, F. Jérôme, Sequential acid-catalyzed alkyl  
456 glycosylation and oligomerization of unprotected carbohydrates, *Green Chem.* 23 (2021)  
457 1361–1369. <https://doi.org/10.1039/d0gc04198j>.
- 458 [29] H.T. Davis, Factors determining emulsion type: Hydrophile-lipophile balance and beyond,  
459 *Colloids Surfaces A Physicochem. Eng. Asp.* 91 (1994) 9–24. [https://doi.org/10.1016/0927-](https://doi.org/10.1016/0927-7757(94)02929-6)  
460 [7757\(94\)02929-6](https://doi.org/10.1016/0927-7757(94)02929-6).
- 461 [30] D.J. McClements, Advances in edible nanoemulsions: Digestion, bioavailability, and  
462 potential toxicity, *Prog. Lipid Res.* 81 (2021) 101081.  
463 <https://doi.org/10.1016/j.plipres.2020.101081>.
- 464 [31] P.G. Argudo, L. Spitzer, F. Jerome, H. Cramail, L. Camacho, S. Lecommandoux, Design  
465 and Self-Assembly of Sugar-Based Amphiphiles: Spherical to Cylindrical Micelles,  
466 *Langmuir.* (2022). <https://doi.org/10.1021/acs.langmuir.2c00579>.
- 467 [32] L. Fernández-Peña, S. Gutiérrez-Muro, E. Guzmán, A. Lucia, F. Ortega, R.G. Rubio, Oil-  
468 in-water microemulsions for thymol solubilization, *Colloids and Interfaces.* 3 (2019).  
469 <https://doi.org/10.3390/colloids3040064>.
- 470 [33] M.K. Nagarajan, J.P. Shah, Conformation and phase transitions in monolayers of some C18  
471 fatty acids containing a hydratable functional group in their alkyl chains, *J. Colloid*  
472 *Interface Sci.* 80 (1981) 7–19. [https://doi.org/10.1016/0021-9797\(81\)90154-5](https://doi.org/10.1016/0021-9797(81)90154-5).
- 473 [34] A. Bhadani, K. Iwabata, K. Sakai, S. Koura, H. Sakai, M. Abe, Sustainable oleic and stearic  
474 acid based biodegradable surfactants, *RSC Adv.* 7 (2017) 10433–10442.  
475 <https://doi.org/10.1039/C6RA27036K>.
- 476 [35] T. Gaudin, H. Lu, G. Fayet, A. Berthault-Drelich, P. Rotureau, G. Pourceau, A.  
477 Wadouachi, E. Van Hecke, A. Nesterenko, I. Pezron, Impact of the chemical structure on  
478 amphiphilic properties of sugar-based surfactants: A literature overview, *Adv. Colloid*  
479 *Interface Sci.* 270 (2019) 87–100. <https://doi.org/10.1016/j.cis.2019.06.003>.
- 480 [36] D.J. McClements, *Food Emulsions*, CRC Press, 2004.  
481 <https://doi.org/10.1201/9781420039436>.
- 482 [37] D. Diwan, K. Shinkai, T. Tetsuka, B. Cao, H. Arai, T. Koyama, K. Hatano, K. Matsuoka,  
483 Synthetic assembly of mannose moieties using polymer chemistry and the biological

- 484 evaluation of its interaction towards concanavalin a, *Molecules*. 22 (2017).  
485 <https://doi.org/10.3390/molecules22010157>.
- 486 [38] Z. Ma, Y.G. Jia, X.X. Zhu, Glycopolymers Bearing Galactose and Betulin: Synthesis,  
487 Encapsulation, and Lectin Recognition, *Biomacromolecules*. 18 (2017) 3812–3818.  
488 <https://doi.org/10.1021/acs.biomac.7b01106>.
- 489 [39] L.M.B. Anaya, R. Petitdemange, M. Rosselin, E. Ibarboure, B. Garbay, E. Garanger, T.J.  
490 Deming, S. Lecommandoux, Design of Thermoresponsive Elastin-Like Glycopolypeptides  
491 for Selective Lectin Binding and Sorting, *Biomacromolecules*. 22 (2021) 76–85.  
492 <https://doi.org/10.1021/acs.biomac.0c00374>.
- 493 [40] H. Brognaro, S. Falke, C.N. Mudogo, C. Betzel, Multi-step concanavalin a phase separation  
494 and early-stage nucleation monitored via dynamic and depolarized light scattering, *Crystals*.  
495 9 (2019). <https://doi.org/10.3390/cryst9120620>.
- 496 [41] N. Vinson, Y. Gou, C.R. Becer, D.M. Haddleton, M.I. Gibson, Optimised “click” synthesis  
497 of glycopolymers with mono/di- and trisaccharides, *Polym. Chem.* 2 (2011) 107–113.  
498 <https://doi.org/10.1039/c0py00260g>.
- 499 [42] W. Wang, S. Tian, X. Jiang, S. Pang, H. Shi, M. Fan, Z. Wang, W. Jiang, W. Hu, X. Xiao,  
500 R. Lin, Molecular Imaging of *Ulex Europaeus* Agglutinin in Colorectal Cancer Using  
501 Confocal Laser Endomicroscopy (With Video), *Front. Oncol.* 11 (2021) 1–9.  
502 <https://doi.org/10.3389/fonc.2021.792420>.
- 503 [43] B. Dumat, L. Montel, L. Pinon, P. Matton, L. Cattiaux, J. Fattaccioli, J.M. Mallet,  
504 Mannose-Coated Fluorescent Lipid Microparticles for Specific Cellular Targeting and  
505 Internalization via Glycoreceptor-Induced Phagocytosis, *ACS Appl. Bio Mater.* 2 (2019)  
506 5118–5126. <https://doi.org/10.1021/acsabm.9b00793>.
- 507 [44] Y. Wang, G. Yu, Z. Han, B. Yang, Y. Hu, X. Zhao, J. Wu, Y. Lv, W. Chai, Specificities of  
508 *Ricinus communis* agglutinin 120 interaction with sulfated galactose, *FEBS Lett.* 585  
509 (2011) 3927–3934. <https://doi.org/10.1016/j.febslet.2011.10.035>.
- 510 [45] J.R. Jass, L.J. Allison, S.M. Stewart, M.R. Lane, *Ulex europaeus* agglutinin-1 binding in  
511 hereditary bowel cancer, *Pathology*. 25 (1993) 114–119.  
512 <https://doi.org/10.3109/00313029309084782>.

514 **Graphical abstract**



515